ACTA ASTRONOMICA
Vol. **68** (2018) pp. 141–158

GT Ursae Majoris AB – a Possible Quadruple System*

W. Dimitrov[1], T. Tomov[2], K. Kamiński[1], M. Polińska[1], I. Iliev[3] and M.K. Kamińska[1]

[1] Astronomical Observatory Institute, Faculty of Physics, A. Mickiewicz University, ul. Słoneczna 36, 60-286 Poznań, Poland
e-mail: dimitrov@amu.edu.pl
[2] Centre for Astronomy, Faculty of Physics, Astronomy and Informatics, Nicolaus Copernicus University, Grudziądzka 5, PL-87-100 Toruń, Poland
[3] Institute of Astronomy, Bulgarian Academy of Sciences, P.O.Box 136, BG-4700 Smolyan, Bulgaria

Received December 12, 2017

ABSTRACT

We present the first spectroscopic study of an eclipsing system GT UMa. Our spectra show that the main visual component A is a triple-lined star, which consists of a close eclipsing pair and a farther third component. Radial velocity measurements show evidence of reflex motion. We used Hipparcos and our own *R*-band light curves for the analysis. These results enabled us to calculate absolute parameters of the eclipsing binary system: 1.37 $M_\odot$ and 1.31 $M_\odot$ and corresponding radii 2.11 $R_\odot$ and 1.63 $R_\odot$. Both eclipsing components are evolved. The orbital period of the eclipsing subsystem is 1.2 d and the semi-major axis – 6.5 $R_\odot$. The wide orbit has low radial velocity amplitude and its parameters are difficult to determine. We obtained a preliminary solution which must be confirmed with future observations. The preliminary period of the wide orbit is 394 d and the lower limit for the semi-major axis – 174 $R_\odot$ (0.81 a.u.). We estimated the mass of the third body to about 1.1 $M_\odot$. Additionally, we investigated the visual companion B. We obtained spectra of this star and measured the radial velocity which is very close to the one of the component A. The proper motions and the parallax are also similar. These are strong arguments that component B is gravitationally bound with the main triple system A.

Key words: *binaries: close – binaries: eclipsing – binaries: spectroscopic – Stars: individual: GT UMa*

1. Introduction

The statistics of stellar multiplicity provide constraints on the initial parameters of the stellar clusters formation. All zero age stars are members of binary or multiple systems. This is confirmed *via* observation and simulations of collapsing molecular clouds (Bate 2004). During dynamical evolution the hierarchy of a

*Based on spectroscopy obtained at the NAO Rozhen, Bulgaria and Poznań Spectroscopic Telescope 1 and 2, Poland

system is established and some lighter components may be ejected from the system. We know more than one hundred multiple stars containing an eclipsing binary (Zashe *et al.* 2009). The existence of an eclipsing pair in the multiple system provides us with a unique possibility to derive precisely the absolute parameters of the components. Most systems are binary or triple and the higher hierarchies are rare (Tokovinin 2014). Observations of multiples are important for understanding of stellar formation, which is still a field of intense investigations (Reipurth 2017, Tholine 2002, Zinnecker 2002). Some of the latest results show processes responsible for creation of multiples. Pineda *et al.* (2015) present observations of core fragmentation responsible for the formation of wide binaries with separations of 10^3-10^4 a.u. Observation of a star forming *via* disk fragmentation were provided by Tobin *et al.* (2016). The separations in this case are about $10^{1.5}-10^{2.5}$ a.u. The most probable mechanism of formation of the closest pairs (10^{-1} a.u.) are the Kozai-Lidov cycles with tidal friction, which causes the orbits to shrink.

Since 2009 we have carried out spectroscopic observations of multiple stars with eclipsing component. Until now the program included three stars: HD 86222 (Dimitrov *et al.* 2014), V342 And (Dimitrov *et al.* 2015) and DY Lyn (Dimitrov *et al.* 2017). We detected new components for all these objects. The main instruments used in this program are small 0.5-m and 0.7-m telescopes equipped with echelle spectrographs, but we also used spectra from 2-m class telescopes.

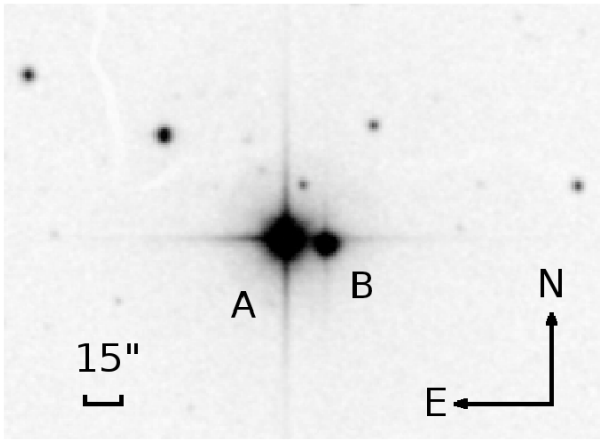

Fig. 1. Direct image of components A and B of GT UMa from the Digital Sky Survey.

The star GT UMa is listed in the Washington Double Star Catalog (WDS – Mason *et al.* 2001) as a visual binary (Fig. 1). The main component A is about 2.6 mag brighter. The equatorial coordinates of the system are $\alpha = 10^{\rm h}35^{\rm m}55\overset{\rm s}{.}7$, $\delta = +63^\circ35'32''$ (FK5). The first light curve and detection of the eclipses comes from Hipparcos satellite. The measured parallax is 6.86 ± 1.18 mas and the corresponding distance is ≈ 122 pc. The star was observed photometrically by Mikuz *et al.* (2004), who improved ephemerides and listed the times-of-minima. The au-

thors presented two ephemerides, the first based on Hipparcos data and the second based on Hipparcos and their photometric observations. Based on the Hipparcos results Mikuz *et al.* (2004) stated that the visual component B is not gravitationally bound to the main star. They noted that the components have very different proper motions. According to the authors, the velocity projected on the plane of the sky is $\gtrsim 200$ km/s and the projected separation between the visual components – 2150 a.u. However, the projected velocity is not consistent with the separation measurements in the last two centuries (Table 1), which showed no significant changes in the angular distance of the two visual components. Therefore, it is likely that component B may be bound to the main star (Section 4).

T a b l e 1

Position angle and separation measurements for GT UMa A and B components from WDS, CCDM

date [yr]	PA	sep.	mag_1	mag_2	Source
1832	268°	$15\farcs0$	–	–	WDS
1909	266°	$17\farcs9$	$8\fm4$	$10\fm8$	CCDM
1991	$266\fdg4$	$17\farcs57$	$8\fm11$	$10\fm65$	Hp., Tyc.
2012	$267\fdg9$	$17\farcs90$	$8\fm17$	$10\fm72$	WDS

(Catalog of the Components of Double and Multiple Stars – Dommagnet and Nys 1994), Hipparcos and Tycho catalogs. The given magnitudes (mag_1 and mag_2) for CCDM and Hipparcos are in visual band, and for WDS the optical part of spectrum.

The most recent measurements of the parallax for GT UMa come from the Tycho-Gaia Astrometric Solution (TGAS – Gaia Collaboration *et al.* 2016, Lindgren *et al.* 2016) catalog: 5.14 ± 0.27 mas (195 ± 10 pc) and Gaia Data Release 2 (Brown *et al.* 2018): 5.05 ± 0.04 mas (198 ± 2 pc). Astrometric results are listed in Table 2.

T a b l e 2

Parallax and proper motion for GT UMa A

source	date [yr]	parallax [mas]	$\mu_\alpha \cdot \cos\delta$ [mas]	μ_δ [mas]
Hipparcos	1997	8.18 ± 1.69	14.30	-9.43
Hipparcos 2nd ed.	1997	6.86 ± 1.18	19.75	-11.59
ASCC	2001	7.88 ± 1.69	16.01	-8.02
Gaia DR1	2015	5.14 ± 0.27	14.04 ± 0.07	-10.28 ± 0.07
Gaia DR2	2018	5.05 ± 0.04	13.99 ± 0.05	-10.62 ± 0.07

The main aim of this paper after the detection of the third component is the determination of the eclipsing binary (EB) pair's parameters and confirmation of the reflex motion visible in the first datasets.

2. Observations

2.1. Detection of the Third Component

The third component was detected at NAO Rozhen with the Coudé spectrograph of the 2-m Ritchey-Chrétien Coudé (RCC) telescope. Since then we have collected spectra at Rozhen with both Coudé and the new Echellé spectrograph (ESPERO), described by Bonev *et al.* (2017). We also have echellé spectra from our two PST[†] telescopes placed in Poland and USA (Arizona). All obtained spectra for GT UMa A are triple-lined (Fig. 2).

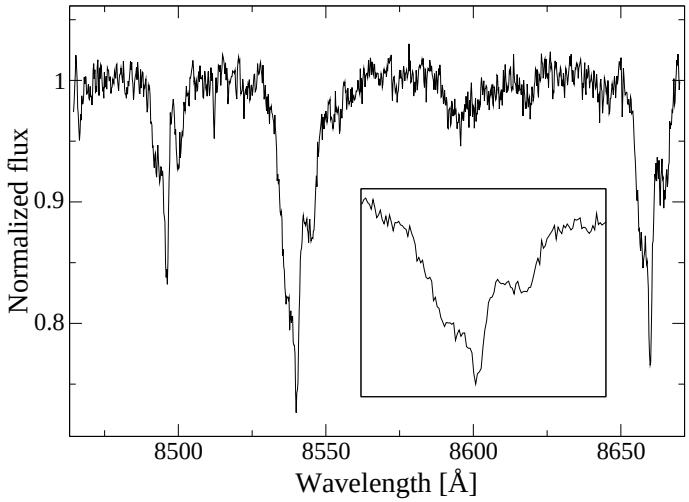

Fig. 2. One of the first Coudé spectra of the GT UMa A star. The triple-lined shape of the near infrared CaII triplet is clearly seen in the inset.

2.2. Radial Velocities

The first data were acquired between December 1999 and December 2003 with the 2 m RCC telescope (Table 3). The Coudé spectrograph equipped with Photometrics CE200A CCD camera was used. The spectra covered a region of about 200 Å around the near infrared CaII triplet with a resolving power of $R \approx 20\,000$. In 2014 we obtained five spectra with the 0.5-m PST1 which indicated that the echellé spectra were more suitable for radial velocity (RV) measurements due to the much longer spectral range. The main dataset was collected with the 0.7-m PST2. The typical signal-to-noise ratio of the spectra is about 20, slightly better in

[†] *http://www.astro.amu.edu.pl/GATS*

the case of PST2. The spectral range for PST1 is 4325–7730 Å and 3880–9180 Å for PST2. Both PST 1/2 spectrographs are fiber-fed, having a resolving power of 35 000 and 40 000, respectively. They are equipped with Andor DZ406 and iKon-L CCD cameras. Part of the data were acquired with ESPERO fiber-fed echellé spectrograph. It is equipped with Andor iKon-L CCD camera. The resolving power of the spectrograph is about 30 000 (Section 4.1).

T a b l e 3

Available spectra and photometry for GT UMa A

Instrument	HJD_{start} -2400000	HJD_{end} -2400000	Time span [d]	n_{obs}	Spectral range [Å] or band
Spectroscopy					
Coudé	51537	52976	1439	40	8464–8670
ESPERO	57210	57476	266	3	3931–9192
PST1	56724	56766	42	5	4325–7730
PST2	56750	57115	365	58	3876–9179
Photometry					
Hipparcos	47875	49053	1178	178	Hp
SPT	53851	53862	11	2268	R

The spectra were reduced using standard IRAF[‡] procedures, including bias, dark, flat-field corrections and spectra extraction with background subtraction. For reduction of PST1 spectra we used IRAF/python scripts and for cosmic ray removal the DCR code (Pych 2004). The PST2 data was reduced with the K. Kamiński code dedicated for this instrument.

The velocities for all the datasets were measured with cross-correlation technique. IRAF FXCOR task was used. We fitted three Gaussian functions to the triple CCF (Cross-Correlation Function) peaks. In Fig. 3 we present the cross-correlation function for different phases. In some cases blending of the three peaks is strong and measurement of the velocities is not possible. We have two broad peaks which correspond to the eclipsing pair components and one narrow, high peak – of the third body. The broadening of the EB peaks results mainly from the short rotational period of the binary. The third body shows significant variations of the RV which could be caused by the reflex motion in the system (Fig. 4). The RV measurements will be available *via* CDS/Vizier database. The shape of the CCF and other parameters are very similar to the previously investigated star in our program – DY Lyn (see Section 3.2).

[‡]IRAF is distributed by the National Optical Astronomy Observatory, which is operated by the Association of Universities for Research in Astronomy, Inc., under a cooperative agreement with the National Science Foundation.

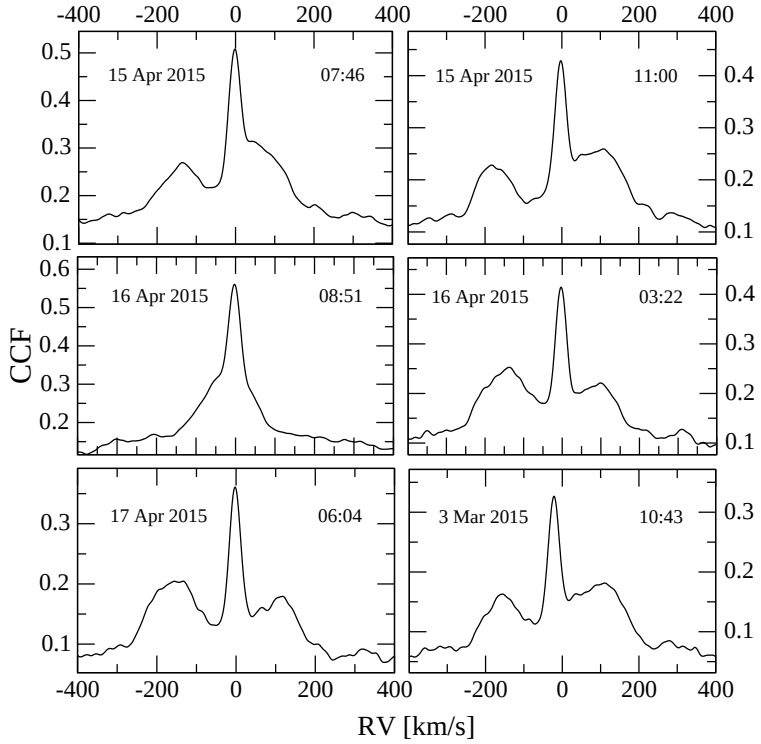

Fig. 3. Three peaks of the cross-correlation functions for GT UMa A in different phases. The date and the Universal Time are given.

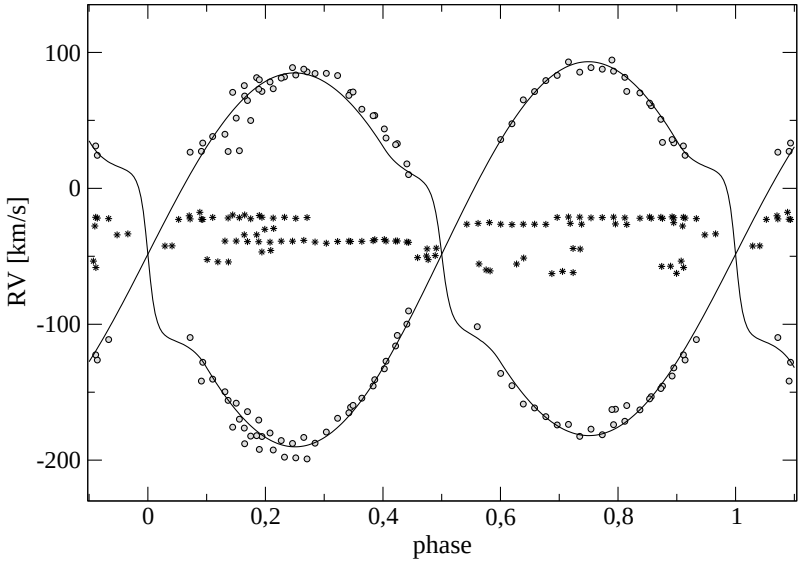

Fig. 4. RV measurements for the three spectroscopic components of GT UMa A phased with the orbital period of the eclipsing pair. RVs of the EB components are marked with open circles while the third component velocities are marked with black dots.

Additionally, we acquired two spectra of the weaker visual component B with ESPERO. Fig. 5 presents the four spectral regions of our spectrum with higher signal-to-noise ratio. The spectrum is typical for the relatively cold main sequence star, the lines are sharp and the Balmer lines have visible wings. The spectrum is analyzed in Section 3.3.

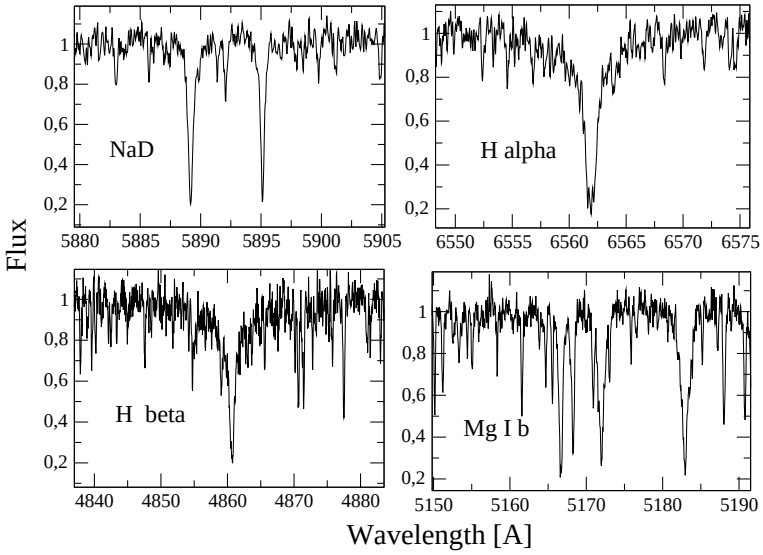

Fig. 5. Four spectral regions of GT UMa B spectrum acquired with ESPERO.

2.3. Light Curves

The light curve from Hipparcos is available, but the scatter is high ($\sigma_{\rm LC} = 0.03$ mag) and the number of points is only 178. We collected new data with a small 20 cm Newton equipped with ST7 SBIG CCD camera and Johnson *R* filter. The new dataset contains 2268 measurements with typical accuracy $\sigma_{\rm LC} = 0.007$.

It is impossible to fit all the data with one period. We have three groups of data spread in time: Hipparcos, our photometric and our RV results. At least one of the datasets is shifted. The times-of-minima and $O-C$ data are listed in Table 4. As the $O-C_1$ residuals show a drift, we calculated a new ephemeris (Eq. 1) which is in a better agreement with the times-of-minima. The corresponding residuals are listed in column $O-C_2$.

$$\mathrm{HJD(MinI)} = 2\,457\,113.25077 + 1\overset{\mathrm{d}}{.}16471430 \cdot E \qquad (1)$$

It is worth noting that new photometric data of GT UMa A are available from ASAS-SN[§] (All-Sky Automated Survey for Supernovae, Shappee *et al.* 2014 and Kochanek *et al.* 2017).

[§] *http://www.astronomy.ohio-state.edu/asassn*

T a b l e 4

Times-of-minima of GT UMa A

HJD −2400000	error [d]	minimum	$O-C_1$ [m]	$O-C_2$ [m]	Cycle	Source
48474.60	0.02	I	20.6	50.7	0	Hipparcos
48738.97	0.02	I	−6.3	21.7	227	Hipparcos
49003.92	0.02	II	−36.7	−10.7	454	Hipparcos
52278.52	0.005	I	−2.9	−2.5	3266	Mikuz *et al.* 2004
52279.69	0.008	I	4.7	5.1	3267	Mikuz *et al.* 2004
52282.60	0.005	II	2.2	2.6	3269	Mikuz *et al.* 2004
52285.51	0.005	I	−0.4	0.0	3272	Mikuz *et al.* 2004
52287.255	0.006	II	−3.3	−3.0	3273	Mikuz *et al.* 2004
52652.396	0.004	I	3.9	1.4	3587	Mikuz *et al.* 2004
52654.72	0.008	I	−3.9	−6.4	3589	Mikuz *et al.* 2004
53851.46711	0.00016	II	10.0	−5.1	4616	photo. R, this paper
53862.53160	0.00020	I	9.7	−12.9	4626	photo. R, this paper
56712.5855	0.0009	I	29.0	−1.8	7073	Hub. and Lehm. (2015)
56756.8516	0.0024	I	39.4	−2.2	7111	RV PST2, this paper
57080.6298	0.0033	I	24.1	4.9	7389	Hubscher (2016)
57113.2623	0.0016	I	53.8	16.6	7417	RV PST2, this paper

Hipparcos minima are taken from Mikuz *et al.* 2004. The two $O-C$ columns are given: $O-C_1$ calculated with respect to the ephemeris presented by Mikuz *et al.* (2004) and $O-C_2$ – from Eq.(1). The deeper minimum is marked as I.

3. Results

3.1. Preliminary Calculations

To prepare for modeling of the system we performed some preliminary calculations. At the beginning we calculated two times-of-minima from the RV data (Table 4). Calculations were done for two phased groups of spectra collected by PST2. There is a phase shift between RV and LC (light curve) of about 0.013, corresponding to about 20 min, which could be caused by the light-time effect of the wide orbit.

The RVs are plotted in Fig. 4. The EB curves (components one and two) have similar amplitudes. The variations of the third body velocity are clearly visible. We fitted the EB RV data and obtained the preliminary parameters presented in Table 5.

Additionally, we made an estimate of temperatures of the three spectroscopic components. We used cross-correlation functions and template spectra with different temperatures to find the one with the best agreement. We obtained temperatures of 6350 ± 100 K, 6400 ± 100 K and 6440 ± 50 K for the first, second and third component, respectively. These values are close to the color temperature of the whole system 6426 K given by Ammons *et al.* (2006). Additionally, we estimated

T a b l e 5

Preliminary fit of the echellé RV results for the close 1.16 d orbit

Parameter	Value
Period [d]	1.164708 fixed
K_1 [km/s]	133.7 ± 1.7
K_2 [km/s]	141.4 ± 1.8
V_γ [km/s]	-48.5 ± 0.7
HJD_0	2457113.8367(17)
σ_{rv} [km/s]	8.2

the ratio of the luminosities of the three stars which is proportional to the surface of Gaussians fitted to the CCF. The more massive EB component has the highest luminosity among the components of GT UMa A: $S_1 : S_2 : S_3 = 0.468 : 0.274 : 0.258$.

3.2. Wide Orbit

The available RV measurements show evidence of reflex motion in the system (Fig. 4). The peak-to-peak amplitude of the third component's RV variation is ≈ 45 km/s. The effect is smaller for the eclipsing pair center of mass (COM) about 15 km/s. The determination of the wide orbit period is difficult due to relatively small number of measurements. For the period analysis we used a code based on the Schwarzenberg-Czerny (1996) method, written by Gracjan Maciejewski (private communication). We have found the best period of about 394 d. The obtained RV curves have significant scatter and the phase coverage is imperfect (Fig. 6). This caused problems with fitting the synthetic curves. We were forced to fix the mass ratio to obtain the result. This parameter was fixed at a value estimated based on a denser group of measurements. Results are listed in Table 6. The substantial scatter of the RV curve for the third component is surprising, because the CCF peak for this component is high and sharp. Dispersion of the subsequent data points obtained during one night is small. Comparing with the very similar data of the previously investigated object DY Lyn we notice that the third body RV curve there has a very low scatter. We searched for alternative periods and for additional variation, *e.g.*, pulsations, which could explain such a big scatter in GT UMa A, but without success. Our results confirm the existence of reflex motion in the system, but precise period and orbital parameters must be confirmed with future observations.

We used the wide orbit results to correct the EB RV data for the reflex motion. The scatter of the corrected data is slightly lower. Both data before and after correction were fitted during modeling of the EB (Section 3.4).

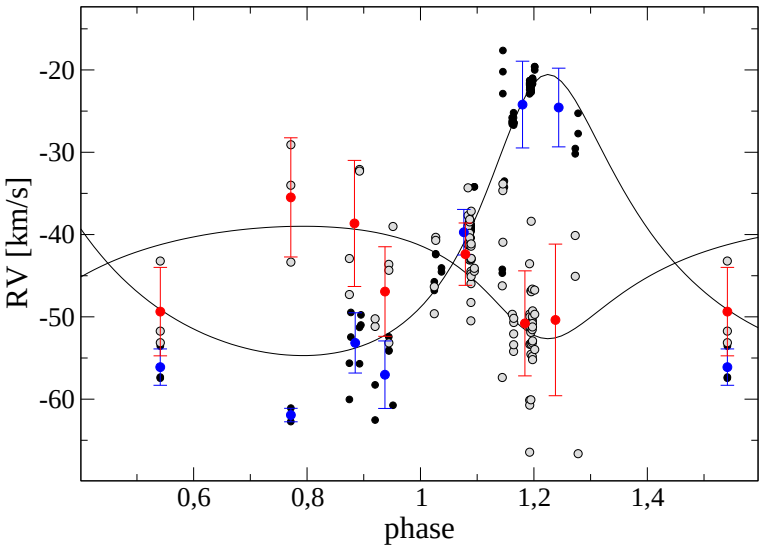

Fig. 6. RV curve for the wide orbit. The results are phased with the 394 d period. RV of the EB-COM are presented with open circles and of the farther third component – with black dots. Red and blue dots represent bins of 0.1 phase.

T a b l e 6

Parameters of the wide orbit derived with PHOEBE

Parameter	Value
P [d]	393.7 ± 0.3
HJD_0	2458262 ± 5
$q = K_3/K_{\mathrm{EB}}$	0.4 fixed
$a \sin i$ [$\mathrm{R}_\odot$]	173.8 ± 12
$a \sin i$ [a.u.]	0.81 ± 0.06
V_γ [km/s]	-43.5 ± 0.4
ω [rad]	2.9 ± 0.2
e	0.36 ± 0.04
K_3 [km/s]	17.1 ± 1.4
K_{EB} [km/s]	6.8 ± 0.6
$m_3 \sin^3 i$ [$\mathrm{M}_\odot$]	0.13 ± 0.04
$m_{\mathrm{EB}} \sin^3 i$ [$\mathrm{M}_\odot$]	0.32 ± 0.11

The errors are formal.

3.3. The Visual Companion GT UMa B

As we mentioned in the Introduction, the question whether the visual component B is dynamically connected with the main system is still open. To solve the problem we acquired two spectra of the B component.

We measured the RV for both spectra using IRAF FXCOR task. The cross-correlation function reveals a sharp, single and symmetric peak (Fig. 7). The he-

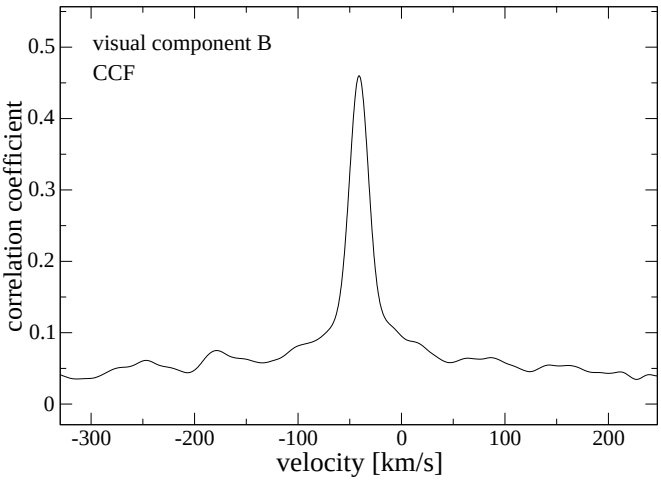

Fig. 7. Sharp, single peak of the GT UMa B CCF.

liocentric values are -41.0 km/s and -40.3 km/s. The time span between the two spectra is about one year. This suggests that the companion is probably single. These values are very close to the systemic velocity of the main visual component, which is -43.5 km/s (Table 6). This is a strong argument that A and B components are dynamically connected.

The ASCC-2.5 (The All-Sky Compiled Catalogue of 2.5 million stars) contains parallaxes for both A and B visual components. They agree within errors, 7.88 ± 1.69 mas for A and 8.40 ± 1.69 mas for B. This is an additional argument that the visual companion is dynamically connected with the main system. Using the same catalog we can calculate the color index for the component B: $B-V = 0.60$ mag. This value corresponds to G1 spectral type and to $T_{\rm eff}$ of about 5850 K. Another source of color measurements is Tycho Double Star Catalogue (TDSC), the color index value listed there is $B-V = 0.584$ mag.

Some catalogs based on TDSC list very high and unrealistic proper motions for component B ($\mu_\alpha = 322.4$ mas/yr and $\mu_\delta = 59.6$ mas/yr). More reliable values are given by the ASCC-2.5: $\mu_\alpha = 19.13$ mas/yr and $\mu_\delta = -9.52$ mas/yr. Those values are close to the proper motion of the component A: $\mu_\alpha = 16.01$ mas/yr and $\mu_\delta = -8.02$ mas/yr and support the hypothesis that the component B may be gravitationally bound to A.

The projected distance between the components A and B is 2560 a.u. This value was calculated for the mean value of the parallax (Table 2) corresponding to the distance of 143 pc and the latest measurement of the angular separation, *i.e.*, $17.''90$ (Table 1).

Atmospheric Parameters of GT UMa B

The spectra of GT UMa B were obtained with the spectrograph ESPERO mounted on the 2-m telescope in Rozhen (Bonev *et al.* 2017). Two spectra in the range from 3900 Å to 9000 Å, with resolving power $R \approx 30\,000$ were taken on July 6,

2015 ($S/N \approx 40$) and on June 21, 2016 ($S/N \approx 60$). We used the second spectrum for the analysis of the atmospheric parameters because of higher S/N. Both spectra had exposure times of 3600 s. The atmospheric parameters: effective temperature $T_{\rm eff}$, surface gravity $\log g$, metallicity [M/H], and projected rotational velocity $v \sin i$ were calculated using the iSPEC[¶] code (Blanco-Cuaresma *et al.* 2014). We assumed microturbulence equal to 1 km/s, macroturbulence 0 km/s and solar abundances (Asplund *et al.* 2009). The observed spectrum was compared with a set of synthetic spectra calculated with the iSPEC code for the ATLAS9 atmospheric models (Kurucz 2005). The atomic data were taken from the VALD database (Kupka *et al.* 2011). First, the effective temperature was estimated using the Balmer lines H_α and H_β. For stars with $T_{\rm eff}$ lower than 8000 K the Balmer lines are not sensitive to $\log g$ (Smalley 2005). Thus, $\log g$ was assumed as 4.0 dex. The effective temperature is 5900 ± 100 K. Comparison of the observed and synthetic spectra of H_β line is shown in Fig. 8. To estimate the error of $T_{\rm eff}$ we took into account the differences in the determined $T_{\rm eff}$ values from separate Balmer lines. For the solar-type stars the surface gravity can be measured from lines which show strong gravity dependence, such as CaI (6162 Å), NaD (5890 Å and 5896 Å), and MgI b (5167 Å, 5172 Å, 5183 Å) (Gray 2005). All the mentioned lines were used to determine $\log g$ of GT UMa B. We assumed $T_{\rm eff}$ equal to 5900 ± 100 K, as obtained from the Balmer lines. The best solution was derived for $\log g = 3.9 \pm 0.2$ dex. As before, the error of $\log g$ was estimated from the differences in the determined $\log g$ values from separate lines. In Fig. 8 observed lines are compared with the computed ones for one of the spectral regions used, *i.e.*, MgI b. Additionally, other parameters of GT UMa B were estimated: metallicity $[M/H] = 0.0 \pm 0.1$ dex and projected rotational velocity $v \sin i = 7.0 \pm 1$ km/s – obtained from spectral lines FeI 6431 Å, FeII 6432 Å, and Ca I 6439 Å, as recommended in Gray (2005). The cross-correlation RV -41 ± 1 km/s was determined with the iSPEC code, using the synthetic spectrum calculated for the derived atmospheric parameters.

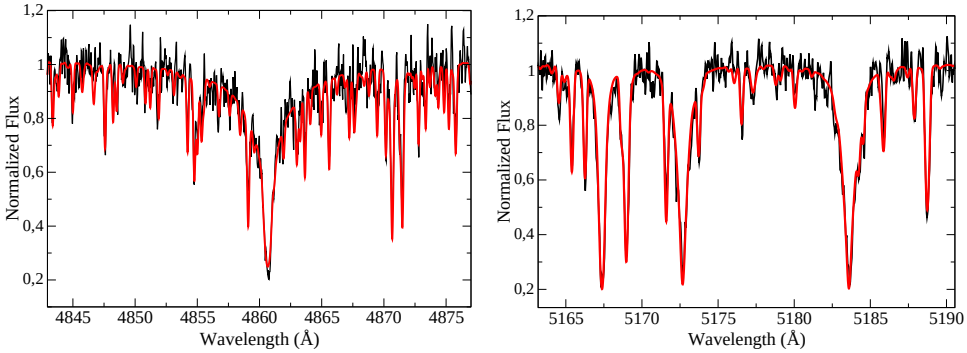

Fig. 8. GT UMa B hydrogen H_β and magnesium triplet lines compared with the fitted model.

[¶]www.blancocuaresma.com/s/iSpec

3.4. Modeling of the Eclipsing Subsystem

We used Wilson-Devinney (W-D) method (Wilson and Devinney 1971) and PHOEBE SVN code (Prša and Zwitter 2005) for modeling of the EB. The EB components are close and distorted, and we assume circular orbit as well as synchronous rotation. We treat the more massive EB component as primary. This star has slightly lower temperature than its close and less massive companion, so the deeper light curve minimum is at phase 0.5 with respect to the ephemeris.

The temperatures of both components are consistent with the convective envelope. We apply gravity brightening coefficients of $g_{12} = 0.32$, and albedos $a_{12} = 0.5$. For calculation of the limb darkening effect we used van Hamme (1993) coefficients and the logarithmic law.

T a b l e 7

GT UMa A model derived with the Wilson-Devinney method for two RV datasets

Parameter	Uncorrected RV data	Corrected RV data	Difference
W-D results			
$i_{\rm EB}$	$80\overset{\circ}{.}03 \pm 0.06$	$80\overset{\circ}{.}18 \pm 0.07$	-0.15
$q_{\rm EB}$	0.950 ± 0.012	0.934 ± 0.011	0.016
$a_{\rm EB}$ [R$_\odot$]	6.470 ± 0.041	6.464 ± 0.038	0.006
Ω_1	4.091 ± 0.008	4.059 ± 0.008	0.032
Ω_2	4.851 ± 0.019	4.820 ± 0.020	0.031
l_1 [R]	0.376 ± 0.003	0.378 ± 0.003	-0.002
l_2 [R]	0.235 ± 0.002	0.231 ± 0.002	0.004
l_3 [R]	0.389 ± 0.003	0.391 ± 0.003	-0.002
l_1 [Hp]	0.379 ± 0.008	0.381 ± 0.008	-0.002
l_2 [Hp]	0.244 ± 0.005	0.238 ± 0.005	0.006
l_3 [Hp]	0.377 ± 0.008	0.381 ± 0.008	-0.004
Absolute parameters			
M_1 [M$_\odot$]	1.373 ± 0.035	1.382 ± 0.032	-0.009
M_2 [M$_\odot$]	1.305 ± 0.033	1.290 ± 0.031	0.005
R_1 [R$_\odot$]	2.111 ± 0.006	2.121 ± 0.005	-0.010
R_2 [R$_\odot$]	1.625 ± 0.014	1.612 ± 0.012	0.013
$T_{\rm eff1}$ [K]	6350 fixed	6350 fixed	–
$T_{\rm eff2}$ [K]	6450 ± 100	6460 ± 100	-10
$M_{\rm bol1}$	2.70 ± 0.07	2.69 ± 0.07	0.01
$M_{\rm bol2}$	3.20 ± 0.08	3.21 ± 0.08	-0.01
$\log g_1$ [cgs]	3.927 ± 0.014	3.926 ± 0.012	0.001
$\log g_2$ [cgs]	4.132 ± 0.018	4.134 ± 0.017	-0.002

Last column presents the difference between the two models.

We used the RV data and *R* and *Hp* band light curves to fit the model of the eclipsing pair. We fit the model for two RV datasets: the original uncorrected and the corrected data (Table 7). The results are very similar and the difference

between them shows how strongly the third body and the reflex motion influence the obtained model. The dispersions of RV measurements are $\sigma_{RV} = 8.1$ km/s and $\sigma_{RV} = 7.5$ km/s for uncorrected and corrected data, respectively. As the wide orbit parameters must be confirmed with future observations, we apply the uncorrected fit as our main result. Our best fit shows two similar components with masses 1.37 $M_\odot$ and 1.31 $M_\odot$. The stars are evolved, the obtained radii are 2.1 $R_\odot$ and 1.6 $R_\odot$. The separation between the stars is only 6.5 $R_\odot$ and the stars are distorted, which is visible in the LC curved maxima.

Our model shows two stars with very similar masses ($q = 0.95$), but with significant difference in radii what is surprising. Both stars are evolved, but component one has larger radii and it is more distorted. It is worth noting that the $\log g$ value for the visual component B is also lower than for main sequence stars (Section 3.3). The primary star temperature was fixed at the value which we obtained using cross-correlation method (Section 3.1). The fitted temperature of the second component is about 100 K higher, as we can expect for the less evolved star with similar mass.

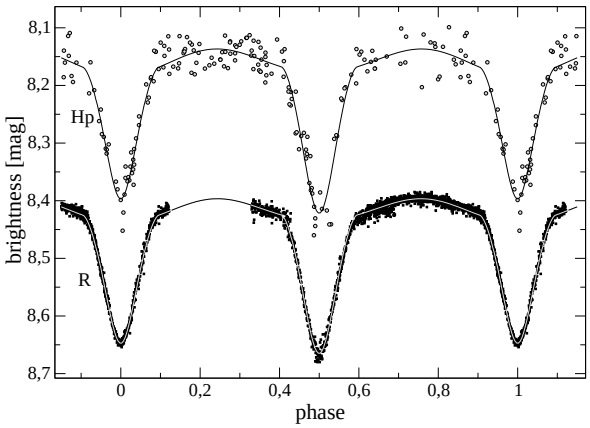

Fig. 9. Photometric measurements and the fitted light curves.

Third Component

The main visual component A is a spectroscopic triple star. It consists of an eclipsing binary (components one and two) and a third component. Here we summarize the results for the third component.

From the W-D model we have the so called "third light" and it is about one third of the light of the A component, 0.39 and 0.38 for *R* and *Hp* filters, respectively. Other estimation of the contribution of the third component in the total flux based on CCF shape suggests lower value of about 26% (Section 3.1). We estimated the temperature of the third component to be 6440 ± 50 K (Section 3.1).

The RV measurements of the third component show peak-to-peak variability of about 45 km/s (Section 3.2). It orbits on a wide orbit around the COM with the close eclipsing pair. Our best fit indicates a period of 394 d and semi-major axis of 173 $R_\odot$. This result must be confirmed with additional RV data, as the

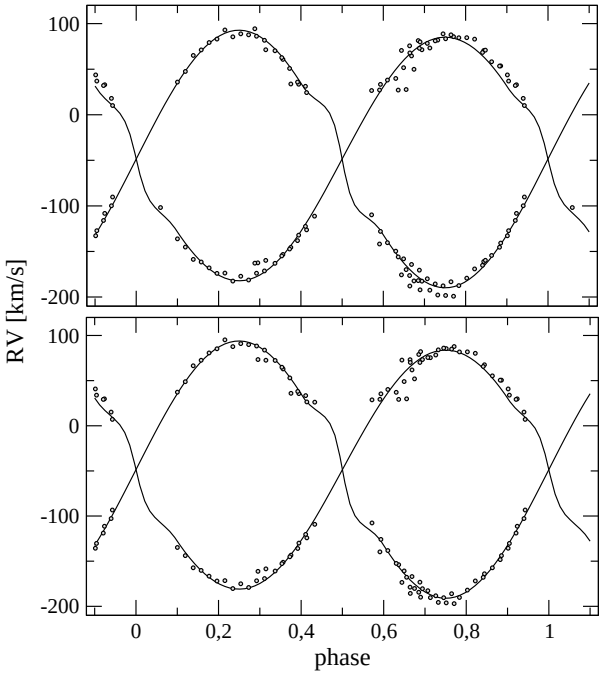

Fig. 10. RV curves for both uncorrected (*upper panel*) and corrected data.

coverage of the phases of the wide orbit is imperfect. The RV curves (Fig. 4) and the amplitudes of the reflex motion suggest that all three spectroscopic components have comparable masses. Using the mass ratio of the wide orbit and EB mass from the W-D model we can estimate the mass of the third body of about 1.07 $M_\odot$.

Alternatively, we can estimate the third mass from the $m_3 \sin^3 i$ (Table 6) and the wide orbit inclination. The obtained result is very close to the previous estimation and it is 1.09 $M_\odot$. We estimated the inclination ($29\overset{\circ}{.}5$) of the wide orbit comparing the $m_{\rm EB} \sin^3 i$ with the mass of the eclipsing binary from the W-D model (Table 7).

Similarity of GT UMa and DY Lyn – the Formation Scenario

One of the objects investigated by our team, DY Lyn (Dimitrov *et al.* 2017), has many similar properties with GT UMa. Both stars consist of main spectroscopically triple system consisting of a close eclipsing pair and a farther third component. The two objects have visual companions. In the case of GT UMa the companion is probably bound with the main system. The angular separation of the visual neighbors is $10''$ and $17''$ for DY Lyn and GT UMa, respectively. The distances to the systems are 198 pc (Gaia DR2) and 285 pc, GT UMa is the closer one. On a first sight the cross-correlation functions of both objects are indistinguishable. Both systems reveal reflex motion which has higher amplitude in the case of DY Lyn. In both cases the eclipsing orbital period is slightly higher than one day (1.3 d for DY Lyn and 1.2 d for GT UMa), and the masses of the eclipsing pairs are

2.35 $M_\odot$ and 2.68 $M_\odot$, respectively. In both cases the mass ratio is very close to one. The dimensions of the close orbits are almost equal – the semi-major axes are 6.5 $R_\odot$ and 6.7 $R_\odot$, the smaller one corresponds to GT UMa. The wide orbit of DY Lyn has a period of 281 d and the projected size of the semi-major axis is 295 $R_\odot$. In the case of GT UMa these values are 394 d and 174 $R_\odot$. We estimated the mass of the third body of 1.4 $M_\odot$ and 1.1 $M_\odot$, respectively. The inclination of the wide orbit of DY Lyn must be close to 90° and about 30° for GT UMa.

Both systems have many common characteristics which suggest a possible similar formation scenario. We could compare the separations between the components with the numerical results of the fragmentation of collapsing clouds. According to Machida *et al.* (2008) the inner part of the systems, the eclipsing pairs, must form in a protostellar epoch of fragmentation. The third components must separate earlier, between the second collapse epoch and the protostellar phase. The far visual companions which are potential fourth components of the systems must form in adiabatic phase. Those components have separations of thousands astronomical units from the main spectroscopically triple systems.

4. Summary and Conclusions

The main result of this paper is the spectroscopic detection of a third component of GT UMa A. The monitoring of the system reveals significant RV changes of the third body caused by reflex motion. The W-D model of the EB subsystem reveals two similar and evolved stars. Models were calculated for two RV datasets: uncorrected and with the correction for reflex motion. The comparison of the two fits reveals that the differences between absolute parameters like mass and radii are less than 1% and the formal errors for both fits are less than 2.5%. Fitting of the wide orbit was difficult and the results must be confirmed with future observations – RV curves have significant dispersion of measurements. In the case of the third component the dispersion is higher than one could expect. This could be caused by some additional variability (pulsation or additional body). Another option is wrong determination of the orbital period. We unsuccessfully searched for alternative periods and additional variability. Solving this problem will be the main aim for future investigation based on new spectroscopic data.

We also observed the potential farther component – the visual companion B. The results suggest that it is likely a member of the GT UMa system. The RV of this component is almost equal with the mean velocity of the EB COM. Additionally, the proper motion and the parallax of A and B components are close to each other. Analysis of the spectrum enabled us to calculate the main atmospheric parameters, like effective temperature, surface gravity $\log g$ and projected rotation $v \sin i$, of the visual companion.

Summing up, our results reveal that GT UMa is a hierarchical quadruple system, consisting of a central spectroscopic triple, seen as component A, which in-

cludes a close eclipsing pair and a more distant neighbor. The visual companion B, which is dynamically connected with component A, is the fourth component of the system.

Acknowledgements. We are grateful to our engineer Roman Baranowski and to Tomasz Kwiatkowski and Alexander Schwarzenberg-Czerny, the founders of the Poznań Spectroscopic Telescope project. This work was supported by the Polish National Science Centre through grant UMO-2011/01/D/ST9/00427. M.P. acknowledges the Polish National Science Center grant no. 2014/13/B/ST9/00902. I.I. acknowledges partial support from the Bulgarian NSF under grants DN-08/01-2016, and DN-18/13-12.12.2017

This work has made use of data from the European Space Agency (ESA) mission Gaia (*http://www.cosmos.esa.int/gaia*), processed by the Gaia Data Processing and Analysis Consortium (*http://www.cosmos.esa.int/web/gaia/dpac/consortium*, DPAC). Funding for the DPAC has been provided by national institutions, in particular the institutions participating in the Gaia Multilateral Agreement.

REFERENCES

Ammons, S.M., Robinson, S.E., Strader, J., Laughlin, G., Fischer, D., and Wolf, A. 2006, *ApJ*, **638**, 1004.
Asplund, M., Grevesse, N., Sauval, A.J., and Scott, P. 2009, *Ann. Rev. Astron. Astrophys.*, **47**, 481.
Bate, M.R. 2004, *Astrophysics and Space Science*, **292**, 297.
Blanco-Cuaresma, S., Soubiran, C., Heiter, U., and Jofré, P. 2014, *A&A*, **569**, A111.
Bonev, T., *et al.* 2017, *Bulgarian Astronomical Journal*, **26**, 67.
Brown, A.G.A., *et al.* 2018, arXiv:1804.09365.
Dimitrov, W., *et al.* 2014, *A&A*, **564**, A26.
Dimitrov, W., *et al.* 2015, *A&A*, **575**, A101.
Dimitrov, W., Lehmann, H., Kamiński, K., Kamińska, M.K., Zgórz, M., and Gibowski, M. 2017, *MNRAS*, **466**, 2.
Dommanget, J., and Nys, O. 1994, *Communications de l'Observatoire Royal de Belgique*, **115**, 1.
Gaia Collaboration Brown, A.G.A., *et al.* 2016, *A&A*, **595**, 2.
Gray, D.F. 2005, in: "The Observation and Analysis of Stellar Photospheres", Cambridge University Press, 2005.
Kochanek, C.S., *et al.* 2017, *PASP*, **129**, 104502.
Kupka, F., and Dubernet, M.-L., VAMDC Collaboration 2011, *Baltic Astronomy*, **20**, 503.
Kurucz, R.L. 2005, *Memorie della Societa Astronomica Italiana Supplementi*, **8**, 14.
Lindegren, L., *et al.* 2016, *A&A*, **595**, 4.
Machida, M.N., Tomisaka, K., Matsumoto, T., and Inutsuka, S. 2008, *ApJ*, **677**, 327.
Mason, B.D., Wycoff, G.L., Hartkopf, W.I., Douglass, G.G., and Worley, C.E. 2001, *AJ*, **122**, 3466.
Mikuz, H., Dintinjana, B., Zwitter, T., and Munari, U. 2004, *IBVS*, 5530.
Pineda, J.E., *et al.* 2015, *Nature*, **518**, 213.
Prša, A., and Zwitter, T. 2005, *ApJ*, **628**, 426.
Pych, W. 2004, *PASP*, **116**, 148.
Reipurth, B. 2017, *Memorie della Societa Astronomica Italiana*, **88**, 611.
Schwarzenberg-Czerny, A. 1996, *ApJ*, **460**, L107.
Shapee, B., J., *et al.* 2014, *ApJ*, **788**, 48S.
Smalley, B. 2005, *Memorie della Societa Astronomica Italiana Supplementi*, **8**, 130.

Tholine, J.E. 2002, *Ann. Rev. Astron. Astrophys.*, **40**, 349.
Tobin, J.J., *et al.* 2016, *Nature*, **538**, 483.
Tokovinin, A. 2014, *AJ*, **147**, 4.
Wilson, R.E., and Devinney, E.J. 1971, *ApJ*, **166**, 605.
van Hamme, W. 1993, *AJ*, **106**, 2096.
Zasche, P., Wolf, M., Hartkopf, W.I., Svoboda, P., Uhlar, R., Liakos, A., and Gazeas, K. 2009, *AJ*, **138**, 664.
Zinnecker, H. 2002, *ASP Conf. Ser.*, **285**, 131.